Edinburgh Research Explorer

Radical polymerization inside living cells

Radical Polymerisation Inside Living Cells

Jin Geng[‡], Weishuo Li[‡], Yichuan Zhang[‡], Neelima Thottappillil, Jessica Clavadetscher, Annamaria Lilienkampf, Mark Bradley*

[‡] These authors contributed equally

EaStCHEM School of Chemistry, University of Edinburgh, Edinburgh, EH9 3FJ UK.

E-mail: mark.bradley@ed.ac.uk

Abstract

Polymerisation reactions conducted inside cells must be compatible with the complex intracellular environment, which contains numerous molecules and functional groups that could potentially prevent or quench polymerisation reactions. Here we report a strategy for directly synthesising unnatural polymers in cells through free radical photo-polymerisation using a number of biocompatible acrylic and methacrylic monomers. This offers a platform to manipulate, track and control cellular behaviour by the *in cellulo* generation of macromolecules that have the ability to alter cellular motility, label cells by the generation of fluorescent polymers for long-term tracking studies, as well as the generation within cells of a variety of nanostructures. It is remarkable that free radical polymerisation chemistry can take place within such complex cellular environments and this demonstration opens up a multitude of new possibilities for how chemists can modulate cellular function and behaviour and for understanding cellular behaviour in response to the generation of free radicals.

Introduction

Synthetic polymers are used extensively in cell biology, from delivery vehicles for DNA and drugs,[1,2] and fluorescent probes for cellular sensing,[3-6] to bioinks for tissue engineering,[7-9] and as polymers that mimic biological functionality, such as artificial antigen presenting

1

cells.[10,11] Typically these polymer constructs are synthesised and formulated before cellular application, although in some cases, such as bioinks, materials are synthesised in the presence of cells.[7-9]

In nature cells are packed with a huge variety of macromolecules that include nucleic acids, proteins and polysaccharides, with the interaction between these macromolecules and small molecules, within the intracellular microenvironment, driving cellular functions, such as cellular motility and differentiation.[12] Microorganisms produce a broad spectrum of biopolymers that include polyphosphates,[13] polyesters, such as poly(hydroxyalkanoates),[14,15] and a variety of polysaccharides, such as chitin,[16] gellan[17] and hyaluronic acid.[18] These clearly have, or display, diverse biological functions, for example as energy storage materials or as surface antigens and virulence factors, while they also have an impact on the mechanical properties of the microorganisms[19] and are attracting attention as a source of biodegradable polymers.[20]

The extracellular formation of polymeric materials for cellular encapsulation[21-26] or the engineering of cell surfaces with macromolecules have been reported,[27-29] but *in cellulo* polymerisation reactions must survive the highly complex intracellular environment that contains a multitude of molecules that might preclude or quench such chemistries. Thus, although the ability to biosynthesise inorganic nanomaterials[30-33] and fluorescent quantum dots[34,35] has been demonstrated in model microorganisms and human cells, to the best of our knowledge, there are no studies demonstrating the free radical mediated intracellular synthesis of non-naturally occurring polymers, nor an understanding of how such polymers alter cellular function, or how they can be used to provide cells with highly robust tracking potential.

Here, we report the first photo-polymerisation approach to generate polymers *in situ* in an intracellular microenvironment, by developing a light-mediated free-radical polymerisation

method using a biocompatible initiator and a range of monomers, with spatial and temporal control of polymerisation under physiological conditions. The polymers generated had a number of cellular effects, such as the promotion of actin polymerisation and impact on cell motility, highly intense fluorescent labelling, while also undergoing intracellular induced polymer aggregation.

Results and discussion

Cytotoxicity and cellular uptake of monomer and initiator

In developing the *in cellulo* polymerisation chemistry (Figure 1a), a benign and cell friendly photo-initiator was required, which was stable in the presence of oxygen and cellular components. 2-Hydroxy-4′-(2-hydroxyethoxy)-2-methylpropiophenone (Irgacure 2959) was selected as the photoinitiator as it has been used in multiple biomedical and tissue engineering applications within aqueous environments and has been shown to be well tolerated by many cell types.[23,36,37] The potential cytotoxicity of acrylate and methacrylate monomers has been previously studied in a number of different cell lines where monomers, such as triethylene glycol dimethacrylate and 2-hydroxyethyl methacrylate, were shown to have toxic effects.[38,39] Thus, our initial studies involved the screening of a variety of monomers and their compatibility in a cellular setting, with HeLa cells incubated with the monomers for 48 h and their IC_{50} values determined. Monomers with low IC_{50} values would clearly not be suitable for intracellular polymerisation, and this included monomers such as poly(ethylene glycol) methacrylate (number-average molecular weight, M_n = 480) and acrylamide, which had IC_{50} values of 1 mM and 1 μM, respectively (see Table 1 for the list of monomers investigated).

We observed no reduction in cell viability and remarkable biocompatibility with the monomers *N*-(2-hydroxypropyl) methacrylamide (HPMA) (up to 250 mM) and sodium 4-

styrenesulfonate (NaSS) (up to 100 mM) after 48 h incubation with HeLa cells. Indeed, HPMA-based polymers have a distinguished record of clinical application,[40] having been used to modify proteins and to aid drug delivery[41,42] due to their excellent biocompatibility and hydrolytic stability.[43] 4-Vinylaniline (VAN) and ferrocenylmethyl methacrylate (FMMA) were also chosen for the intracellular polymerisations (see later) and showed IC_{50} values of 56 mM and 68 mM, respectively. The cellular uptake by HeLa cells was determined by incubation with the monomer and initiator, followed by washing and cell lysis, and subsequent HPLC analysis, which showed cellular uptake of ≈58% and ≈49% for HPMA (50 mM) and Irgacure 2959 (2 mM), respectively, after 4 h incubation (Figure 1c, Supplementary Fig. 13).

Polymerisation conditions

In order to develop robust and biologically suitable conditions for intracellular photo-polymerisation, we examined a number of polymerisation parameters including the concentration of initiator (0.5–5 mM) and monomers (1–100 mM), and the duration of photo-activation (5–15 min) at 362–370 nm (with maximum emission at 365 nm, see Supplementary Fig. 1), with the lamp with an intensity of 5 mW cm^{-2} fixed at 5 cm above the samples. A remarkable cellular tolerance to both the monomers and initiator was found at all tested concentrations, while cells remained viable following illumination for up to 10 min (Supplementary Fig. 20).

The photo-polymerisation of HPMA (Irgacure 2959 as an initiator, 5 min at 365 nm) was initially investigated *in vitro* with a series of concentrations and monomer/initiator ratios under different reaction conditions, including the presence or absence of O_2 in phosphate buffered saline (PBS, pH 7.4) or cell lysate (with and without glutathione (GSH)). Monomer concentrations below 20 mM and initiator concentrations below 600 μM gave no

polymerisation in PBS (as observed by NMR, see supporting information Table S1). Polymerisation of 50 mM HPMA in the presence of Irgacure 2959 (2 mM) with illumination at 365 nm for 5 min at room temperature allowed polymerisation and showed a 48% conversion, giving a polymer with a M_n of 13.5 kDa and a dispersity ($Đ$, defined as the ratio of weight-average molecular weight to M_n) of 1.78 (as determined by gel permeation chromatography (GPC)). Changing the initiator to the equally cytocompatible and more water-soluble BAPO-ONa (Supplementary Fig. 2), gave similar levels of conversion in the polymerisation (supporting information Table S1). The removal of O_2 from the solution had no effect on the conversion. Notably, the polymerisation proceeded equally well in cell lysate with 48% conversion of HPMA (50 mM), despite the presence of free radical scavenging activity of antioxidant systems, such as GSH.[44] Moreover, 50 mM GSH in cell lysate had no detrimental effect on the polymerisation and GSH did not act as chain transfer agent for the polymerisation as evident from ^{1}H NMR (Supplementary Fig. 10), further indicating the biological compatibility of the monomer/initiator system. In cell lysate, the resulting polymers ranged from 15 kDa to 19 kDa, similar to polymers formed in PBS, with the M_n increasing with increasing monomer concentration (from 50 mM to 1 M at 25/1 monomer/initiator ratio) (Supplementary Table 2).

Intracellular polymerisation has no effect on cell viability

Mixtures of Irgacure 2959 (2 mM) and monomer HPMA (1–100 mM) were prepared in complete culture media and added to HeLa cells, followed by incubation for 4 h. The cells were washed, incubated in fresh media, and illuminated with at 365 nm (5 mW cm^{-2}, 5 cm from the target), without significant adverse effects on cell viability at exposure times of 5 min (> 85% cell viability, Figure 1b and Supplementary Fig. 23), in agreement with previous studies that suggested that localised radicals produced in cells are not directly relevant to cell

viability.[23,36] The biocompatibility of polymerisation of HPMA was also observed in ARN8 and PC3 cells, which showed cell viabilities > 90% using the same conditions as described above (Supplementary Fig. 24 and Fig. 25). Importantly, 7 days after polymerisation, there was no reduction in viability or proliferation of the photo-polymerised cells (50 mM HPMA, 2 mM Irgacure 2959, 5 min at 365 nm) compared to treated cells without illumination and untreated cells (Supplementary Fig. 26 and Fig. 27).

Having demonstrated cellular compatibility, the structure of the polymer generated during intracellular polymerisation was explored. The conversion in cells was determined to be *ca* 68% based on the remaining concentration of HPMA in cells after illumination (Figure 1d), as measured from cell lysate (0.06 pmol per polymerised cell *vs* 0.19 pmol per untreated cell), similar to the polymerisation levels carried out in PBS and cell lysate (~ 50% conversion) under the same conditions. No detectable consumption of HPMA was observed in cells in the absence of initiator under illumination at 365 nm (5 min).

To confirm whether the polymerisation was by a free radical mechanism, we detected the radicals produced intracellularly under our experimental conditions by using dichloro-dihydro-fluorescein diacetate (DCFH-DA) assay, which is one of the most widely used techniques for directly measuring free radicals and other reactive oxygen species in cells.[45] Notably higher levels of fluorescence intensity was detected in the cells that were treated with initiator and UV illuminated for 5 min at 365 nm, with or without monomer, compared to both the untreated cells and only UV treated cells (Supplementary Fig. 28). These results indicate that free radicals were produced in cells by the photoinitiator (Irgacure 2959), which is consistent with our result that no polymerisation of HPMA was observed in the absence of the initiator (with or without illumination).

To isolate the polymer from cells, a biotin-PEG methacrylate was used to provide an isolation handle. HeLa cells were incubated for 4 h with biotin-PEG methacrylate (0.1 equivalent to

HPMA) and HPMA (50 mM) in the presence of Irgacure 2959 (2 mM), followed by illumination for 5 min at 365 nm. The cells were harvested, lysed and the polymer isolated using streptavidin functionalised magnetic nanoparticles, allowing isolation of a polymer with a M_n of 12.7 kDa and a $Đ$ of 1.62, with MALDI-TOF MS analysis showing molecular ion intervals indicative of the HPMA repeating units (Supplementary Fig. 31 and Fig. 33).

Intracellular polymerisation affects cell cycle

To gain insight into the effect of photo-induced intracellular polymerisation on cell cycle progression, HeLa cells were treated with HPMA (50 mM) and initiator (2 mM) followed by illumination (5 min at 365 nm) under normal growth conditions with cells analysed at 2 h, 24 h, 48 h, and 72 h by flow cytometry. There were no significant differences in the G_1 and G_2 phases between the treated and untreated cells (Figure 1e and 1g). At 48 h, "polymerised cells" showed a delay in entering the S phase (6% of cells were in S phase in comparison to 12% of untreated cells, $p < 0.05$); however, "polymerised cells" had similar DNA contents after 72 h (Figure 1f). The G_1/S border was not accompanied by an increased apoptotic response following polymerisation in cells (Figure 1h). In addition, there were no notable differences in cell cycle progression comparing cells with and without illumination, meaning that the illumination at 365 nm did not result in any significant DNA damage (Supplementary Fig. 37 – Fig. 40).

Cellular mechanics and the cytoskeleton

Intracellular polymerisation changes cell migration modes

To investigate the role intracellular polymers play in altering cellular migration, a wound healing migration assay was used. The percentage of wound closure in untreated cells and "polymerised cells" was similar over 24 h (67% for both), whereas after 48 h and 72 h the

polymerised cells showed a significantly reduced motility compared to untreated HeLa cells (Figure 2). The "polymerised cells" presumably migrated more slowly as a consequence of the acquired internal polymer resulting in a phenotype that has altered cell body translocation.[46,47] It is worth noting that we did not observe any significant differences between cells that were untreated with and without illumination, and HPMA and initiator treated but without illumination at 365 nm. Moreover, we observed that cell motility could be manipulated by cellular polymerisation using different ratios of monomer and initiator, with lower initiator concentrations resulting in slower migration of cells. Thus, a monomer to initiator ratio of 125:1 (250 mM and 2 mM, respectively) gave a gap of 62% after 72 h, whereas with a ratio of 25:1 (50 mM and 2 mM, respectively) and 50:1 (100 mM and 2 mM, respectively) gaps of 25% and 29%, respectively, compared to 0% for untreated cells (Supplementary Fig. 41). As discussed above, there was no significant change in cell proliferation for the "polymerised cells" compared to the untreated cells (Supplementary Fig. 27), but the formation of polymers inside the cells did modify their migration abilities.

Actin filament ordering increases after intracellular polymerisation

Since polymerisation inside a cell would increase cellular viscosity, it may trigger actin polymerisation[48] as well as the demonstrated changes in migratory behaviour. Although it is still challenging to measure the cellular forces,[49] internally generated physical forces can act through the cytoskeleton to affect the local mechanical properties and hence cellular behaviour.[50,51] As such, the actin organisation in individual cells upon intracellular polymerisation could have an effect similar to actin binding and crosslinking proteins.[52-54]

To better understand how intracellular polymerisation alters actin polymerisation, F-actin staining and actin reorganisation were analysed. The local angles of actin filaments within untreated HeLa cells (with and without illumination for 5 min at 365 nm) and "polymerised

cells" were analysed and are represented as coloured orientation plots in Figure 3.[55] Marked differences in the cellular structure of "polymerised cells" were observed with a well-spread phenotype and a polarised morphology compared to untreated cells. Without polymerisation, the observed cell shape correlated with an orthoradial actin distribution, together with small adhesion complexes mostly distributed at the cell edge (Figure 3a and 3b). In comparison to untreated cells (with and without illumination), the actin stress fibres in the "polymerised cells" appeared to cluster into large locally ordered microdomains shown by their uniform orientation distribution (Figure 3c). In addition, the cell area containing microdomains increased and cells were more elongated (Figure 3e). Anisotropy of the actin was quantified using the FibrilTool[56] and showed significantly higher anisotropy values for "polymerised cells" after 72 h when compared to untreated cells with and without illumination ($p < 0.05$) (Figure 3f).

Polymerisation induced fluorescence enhancement in cells

Having demonstrated intracellular polymerisation with HPMA, we sought to expand the approach to more challenging polymers with greater practical applications. Biomacromolecule-based fluorophores are well retained in cells over multiple passages, in comparison to small molecule dyes[57] and, thus, we targeted the *in situ* generation of fluorescent polymers.

Polymerisation of sodium 4-styrenesulfonate (NaSS) is known to generate fluorescent polymers (supporting information Supplementary Fig. 42).[58-60] Using the same set of intracellular polymerisation conditions as before, incubation of non-fluorescent NaSS (50 mM) and Irgacure 2959 (2 mM) with HeLa cells followed by 5 min illumination resulted in the intracellular generation of poly(NaSS) localised in the cytoplasm (determined by confocal

microscopy, Figure 4). There was a shift of the whole cell population towards higher fluorescence intensity when compared to untreated cells as observed by flow cytometry (Supplementary Fig. 46). Likewise, polymerisation of 4-vinylaniline (VAN) generated intracellular fluorescent polymers in HeLa cells. The poly(VAN) was predominantly localised in lysosomes[61] perhaps driven by poly(VAN) protonation (pKa = 4.6) (Supplementary Fig. 47). [62,63]

To increase the overall fluorescence intensity of the *in situ* synthesised polymer and allow analysis over multiple cell passages, rhodamine B acrylate (acryloxyethyl thiocarbamoyl rhodamine B (AOTCRhB)) was used to create a co-polymer with HPMA inside cells (a co-polymer was used as AOTCRhB was toxic to cells at high concentration (IC$_{50}$ = 20 µM)). Thus, HeLa cells were incubated with HPMA (20 mM) and AOTCRhB (5 µM) and initiator (1 mM) for 4 h and, following washing, photo-polymerisation was initiated. Cells were grown for five passages and analysed by flow cytometry and fluorescence microscopy at each passage (Supplementary Fig. 48). Following polymerisation, the fluorescence intensity of the cells increased dramatically in comparison to untreated cells and cells treated with monomers but no illumination (some 100-fold increase at P1 compared to untreated cells) (Figure 5b and Supplementary Fig. 49). After five passages, the fluorescence intensity naturally reduced; however, the "polymerised cells" still exhibited high fluorescence intensity when compared with non-polymerised cells. This long-term retention of fluorescence within the "polymerised cells" suggests that intracellular polymerisation is a viable strategy for creating long-term cellular tracking reporters, an important requirement in regenerative medicine where there is powerful need to track implanted cells.

Polymerisation induced intracellular polymer aggregation

As a final example of intracellular polymerisation, ferrocenylmethyl methacrylate (FMMA) was used. The polymerisation of FMMA (10 mM) was initially explored in PBS in the presence of the initiator (1 mM) with 5 min illumination. GPC analysis showed a polymer with M_n of 6.2 kDa and a Đ of 1.52, which aggregated into nanoparticles *in situ* presumably as a consequence of the polymer precipitating (Figure 5b).

HeLa cells were incubated with FMMA (10 mM) and initiator (1 mM), and polymerised as above. Transmission electron microscopy (TEM) showed the *in situ* generation of nanoparticles within cells with spherical features of around 50–70 nm in diameter in both the cytoplasm and nucleus, similar to the dimensions of the poly(FMMA) aggregates found in PBS (Figure 5 and Supplementary Fig. 51). Cells treated with FMMA and initiator without illumination showed no such structures, which was in agreement with control experiments where FMMA monomer showed no nanostructures in PBS (Supplementary Fig. 50).

Previous studies have shown that ferrocene-conjugated small molecules have the ability to enter the cell nucleus.[64,65] By contrast, ferrocene-based polymers[66] and nanoparticles[67] have only been found in the cytoplasm. Taken together, our results suggest that the FMMA crossed not just the cellular membrane, but also the nuclear membrane, and was polymerised (under illumination) and aggregated *in situ*. 2-Hydroxyethyl methacrylate (HEMA) and *O*-2-hyroxypropyl methacrylate (*O*-HPMA), which are known to be polymerised into water insoluble polymers,[68,69] were also photo-polymerised in cells under the same conditions. TEM analysis showed polymer aggregates inside cells after the *in cellulo* polymerisation of HEMA or *O*-HPMA (Supplementary Fig. 54).

Conclusions

Being able to use light-mediated polymerisation to generate new-to-nature polymers in live cells paves the way for intracellular engineering in which the functional polymers formed *in*

situ can be explored in fluorescence imaging, controlling cytoskeleton function and cellular motility. The ability to generate free radicals within the cellular environment and to use them to generate polymers also raises many questions about the mechanisms of free radical scavenging chemistries within cells. The potential power and applicability of this approach allows us to expand the toolkit of cytocompatible chemistries into intracellular synthetic macromolecules and further exploration into the realm of intracellular polymerisation promises to be a great adventure.

Methods

Cell culture. HeLa cells were maintained in Dulbecco's Modified Eagle's Medium (DMEM), supplemented with 10 % (*v/v*) fetal bovine serum (FBS) and penicillin/streptomycin (100 U/mL of each), in a cell incubator (37 °C and 5 % CO_2). The cells were regularly passaged using trypsin/EDTA.

General procedure for intracellular polymerisation. HeLa cells were seeded in a 96-well plate at a density of 1×10^5 cells per well and cultured overnight. The cells were then treated with monomer HPMA (50 mM) and Irgacure 2959 (2 mM) for 4 h. The cells were washed with PBS (3 × 200 µL) and fresh medium added (200 µL). Polymerisation was initiated by illumination at 365 nm for 5 min, with the lamp fixed 5 cm above the plate. The cells were incubated at 37 °C for further examinations. Polymerisation of other monomers typically followed the same procedure. Untreated cells were used as a control, unless otherwise stated.

Cell cycle study. HeLa cells were seeded in 24-well plate at a density of 5×10^4 cells per well and incubated at 37 °C overnight. To each well, HPMA (50 mM) and Irgacure 2959 (2 mM) were added and incubated at 37 °C for 4 h, followed by washing and polymerisation as described above. The cells were then incubated at 37 °C for 48 h. The media was removed and the cells were gently washed twice with PBS. The cells were treated with 1% trypsin

(200 µL) for 10 min and the detached cells were suspended in fresh media (800 µL) and transferred to test tubes. To each tube, Vybrant® DyeCycle^{TM} Green (2 µL of a 5 mM stock solution) was added and incubated for 30 min in dark. The samples were analysed on a flow cytometer using a FITC filter (λ_{ex} = 488 nm).

Cell motility study. HeLa cells were seeded in Ibidi® Culture-Insert 2 Well µ-Dish at a density of 1.5×10^4 cell per well (in 70 µL media) and incubated at 37 °C overnight. To each well, HPMA (3.5 µL of a 1 M stock solution) and Irgacure 2959 (7.0 µL of a 20 mM stock solution) was added and incubated at 37 ˚C for 4 h, followed by gentle washing with PBS (3 × 70 µL). Fresh media (70 µL) was added and the plate with cells was illuminated for 5 min from the top. Cell Tracker Red® (0.7 µL of a 1 mM stock solution) was added to each well and incubated at 37 ˚C for 30 min. The media was removed and the cells were gently washed three times with PBS. The PBS was decanted and the insert modes were removed, followed by addition of fresh media (2 mL) to the dish. Microscopy images were taken using the GFP channel (λ_{ex} = 475 nm, λ_{em} = 509 nm) and the bright field channel every 24 h and the diameter of the void between cells measured using ImageJ with the Wound Healing Tool plugin, using the variance method.

Actin staining and measurement of actin filament orientation. HeLa cells were seeded onto polylysine coated glass slides placed on a 24-well plate at a density of 1×10^4 cells and incubated overnight. HPMA (50 mM) and Irgacure 2959 (2 mM) were added to the medium and the cells incubated at 37 °C for 4 h, followed by washing and polymerisation as described above. After 48 h and 72 h incubation at 37 °C, cells were washed three times with PBS and stained with Alexa Fluor™ 488 Phalloidin following the manufacturer's instructions, and images (λ_{ex} = 475 nm, λ_{em} = 509 nm) were taken by confocal laser scanning microscopy. The images of cells with fluorescently labelled actin filaments were analysed using ImageJ with OrientationJ plugin and the anisotropy of actin was quantified using FibrilTool.

Measurement of actin area. Images of fluorescently labelled cells were smoothed using a Gaussian filter in ImageJ, followed by removal of the background using a 20 μm diameter rolling ball. The images were then thresholded and the actin microdomains were analysed to obtain the area.

Cell passage study. HeLa cells were seeded in 6-well plate at a density of 1×10^5 cells per well and incubated at 37 °C overnight. To each well, acryloxyethyl thiocarbamoyl rhodamine B (50 μM), HPMA (20 mM) and Irgacure 2959 (2 mM) were added and incubated at 37 °C for 4 h, followed by washing and polymerisation as described above. For each passage analysis, cells were treated with 1% trypsin (500 μL) for 10 min and the detached cells were suspended in fresh media. Cell suspensions were transferred to cytometry tubes and analysed on a flow cytometer using a PI filter (λ_{ex} = 586 nm). The rest of the cells were seeded back into new well plate (1×10^5 cells per well) and incubated at 37 °C. The trypsinisation process, microscopy imaging and flow cytometry analysis were repeated every 48 h for 5 passages.

References

1. Nicolas, J., Mura, S., Brambilla, D., Mackiewicz, N. & Couvreur, P. Design, functionalization strategies and biomedical applications of targeted biodegradable/biocompatible polymer -based nanocarriers for drug delivery. *Chem. Soc. Rev.* **42,** 1147–1235 (2013).

2. Green, J. J. & Elisseeff, J. H. Mimicking biological functionality with polymers for biomedical applications. *Nature* **540,** 386–394 (2016).

3. Howes, P. D., Chandrawati, R. & Stevens, M. M. Colloidal nanoparticles as advanced biological sensors. *Science* **346,** 1247390 (2014).

4. Tang, F., He, F., Cheng, H. & Li, L. Self-Assembly of Conjugated Polymer-Ag@SiO 2Hybrid Fluorescent Nanoparticles for Application to Cellular Imaging. *Langmuir* **26,** 11774–11778 (2010).

5. Tonga, G. Y. *et al.* Supramolecular regulation of bioorthogonal catalysis in cells using nanoparticle-embedded transition metal catalysts. *Nat. Chem.* **7,** 597–603 (2015).

6. Yusop, R. M., Unciti-Broceta, A., Johansson, E. M. V., Sanchez-Martin, R. M. & Bradley, M. Palladium-mediated intracellular chemistry. *Nat. Chem.* **3,** 239–243 (2011).

7. Collins, M. N. & Birkinshaw, C. Hyaluronic acid based scaffolds for tissue engineering—A review. *Carbohyd. Polym.* **92,** 1262–1279 (2013).

8. Tasoglu, S. & Demirci, U. Bioprinting for stem cell research. *Trends Biotechnol.* **31,** 10–19 (2013).

9. Hutmacher, D. W. Scaffolds in tissue engineering bone and cartilage. *Biomaterials* **21,** 2529–2543 (2000).

10. Meyer, R. A. *et al.* Biodegradable nanoellipsoidal artificial antigen presenting cells for antigen specific T-cell activation. *Small* **11,** 1519–1525 (2015).

11. Hu, C.-M. J. *et al.* Erythrocyte membrane-camouflaged polymeric nanoparticles as a biomimetic delivery platform. *P. Natl. Acad. Sci. USA* **108,** 10980–10985 (2011).

12. Lodish, H. *et al. Molecular Cell Biology*. (W H Freeman & Company, 2007).

13. Zhu, Y., Huang, W., Lee, S. S. K. & Xu, W. Crystal structure of a polyphosphate kinase and its implications for polyphosphate synthesis. *EMBO reports* **6,** 681–687 (2005).

14. Anderson, A. J., Haywood, G. W. & Dawes, E. A. Biosynthesis and composition of bacterial poly(hydroxyalkanoates). *Int. J. Biol. Macromolec.* **12,** 102–105 (1990).

15. Kessler, B. & Witholt, B. Factors involved in the regulatory network of polyhydroxyalkanoate metabolism. *J. Biotechnol.* **86,** 97–104 (2001).

16. Adams, D. J. Fungal cell wall chitinases and glucanases. *Microbiology* **150,** 2029–2035 (2004).

17. Arakawa, Y. *et al.* Genomic organization of the Klebsiella pneumoniae cps region responsible for serotype K2 capsular polysaccharide synthesis in the virulent strain Chedid. *J. Bacteriol* **177,** 1788–1796 (1995).

18. Chien, L. J. & Lee, C. K. Enhanced hyaluronic acid production in bacillussubtilis by coexpressing bacterial Hemoglobin. *Biotechnol. Progr.* **23,** 1017–1022 (2007).

19. Brangwynne, C. P., Tompa, P. & Pappu, von, R. Polymer physics of intracellular phase transitions. *Nat. Phys.* **11,** 899–904 (2015).

20. Rehm, B. H. A. Bacterial polymers: biosynthesis, modifications and applications. *Nat. Rev. Microbiol.* **8,** 578–592 (2010).

21. Yang, S. H. *et al.* Mussel-inspired encapsulation and functionalization of individual yeast cells. *J. Am. Chem. Soc.* **133,** 2795–2797 (2011).

22.   Tytgat, L. *et al.* in *3D Printing and Biofabrication* **96,** 1–43 (Springer International Publishing, 2017).

23.   Williams, C. G., Malik, A. N., Kim, T. K., Manson, P. N. & Elisseeff, J. H. Variable cytocompatibility of six cell lines with photoinitiators used for polymerizing hydrogels and cell encapsulation. *Biomaterials* **26,** 1211–1218 (2005).

24.   Yang, J. *et al.* Nanoencapsulation of individual mammalian cells with cytoprotective polymer shell. *Biomaterials* **133,** 253–262 (2017).

25.   Xia, Y. *et al.* Photopolymerized injectable water-soluble maleilated chitosan/ poly(ethylene glycol) diacrylate hydrogels as potential tissue engineering scaffolds. *J. Photopol. Sci. Technol.* **30,** 33–40 (2017).

26.   Pathak, C. P., Sawhney, A. S. & Hubbell, J. A. Rapid Photopolymerization of Immunoprotective Gels in Contact with Cells and Tissue. *J. Am. Chem. Soc.* **114,** 8311–8312 (1992).

27.   Magennis, E. P. *et al.* Bacteria-instructed synthesis of polymers for self-selective microbial binding and labelling. *Nat. Mater.* **13,** 748–755 (2014).

28.   Kim, J. Y. *et al.* Cytocompatible Polymer Grafting from Individual Living Cells by Atom-Transfer Radical Polymerization. *Angew. Chem. Int. Edit.* **55,** 15306–15309 (2016).

29.   Niu, J. *et al.* Engineering live cell surfaces with functional polymers via cytocompatible controlled radical polymerization. *Nat. Chem.* **9,** 537–545 (2017).

30.   Ma, X. *et al.* Construction and Potential Applications of a Functionalized Cell with an Intracellular Mineral Scaffold. *Angew. Chem. Int. Edit.* **50,** 7414–7417 (2011).

31.   Sweeney, R. Y. *et al.* Bacterial biosynthesis of cadmium sulfide nanocrystals. *Chem. Biol.* **11,** 1553–1559 (2004).

32.   Klaus, T., Joerger, R., Olsson, E. & Granqvist, C.-G. Silver-based crystalline nanoparticles, microbially fabricated. *P. Natl. Acad. Sci. USA* **96,** 13611–13614 (1999).

33.   Said, El, W. A., Cho, H. Y., Yea, C. H. & Choi, J. W. Synthesis of metal nanoparticles inside living human cells based on the intracellular formation Process. *Adv. Mater.* **26,** 910–918 (2014).

34.   Li, Y. *et al.* Mechanism-oriented controllability of intracellular quantum dots formation: the role of glutathione metabolic pathway. *Acs Nano* **7,** 2240–2248 (2013).

35.   Cui, R. *et al.* Living yeast cells as a controllable biosynthesizer for fluorescent quantum dots. *Adv. Funct. Mater.* **19,** 2359–2364 (2009).

36. Bryant, S. J., Nuttelman, C. R. & Anseth, K. S. Cytocompatibility of UV and visible light photoinitiating systems on cultured NIH/3T3 fibroblasts in vitro. *J. Biomat. Sci. Polym. Edit.* **11,** 439–457 (2000).

37. Fedorovich, N. E. *et al.* The effect of photopolymerization on stem cells embedded in hydrogels. *Biomaterials* **30,** 344–353 (2009).

38. Schweikl, H., Spagnuolo, G. & Schmalz, G. Genetic and cellular toxicology of dental resin monomers. *J. Dent. Res.* **85,** 870–877 (2006).

39. Issa, Y., Watts, D. C., Brunton, P. A., Waters, C. M. & Duxbury, A. J. Resin composite monomers alter MTT and LDH activity of human gingival fibroblasts in vitro. *Dent. Mater.* **20,** 12–20 (2004).

40. Vasey, P. A. *et al.* Phase I clinical and pharmacokinetic study of PK1 [N-(2-Hydroxypropyl)methacrylamide copolymer Doxorubicin]: first member of a new class of chemotherapeutic agents—drug-polymer conjugates. *Clin. Cancer Res.* **5,** 83–94 (1999).

41. Callahan, J.Jindřich Kopeček. Semitelechelic HPMA copolymers functionalized with triphenylphosphonium as drug carriers for membrane transduction and mitochondrial localization. *Biomacromolecules* **7,** 2347–2356 (2006).

42. Kopecek, J. & Kopečková, P. HPMA copolymers: origins, early developments, present, and future. *Adv. Drug. Deliver. Rev.* **62,** 122–149 (2010).

43. Lilly, J. L., Romero, G., Xu, W., Shin, H. Y. & Berron, B. J. Characterization of molecular transport in ultrathin hydrogel coatings for cellular immunoprotection. *Biomacromolecules* **16,** 541–549 (2015).

44. Dröge, W. Free Radicals in the physiological control of cell function. *Physiol. Rev.* **82,** 47–95 (2002).

45. Armstrong, D. *Advanced Protocols in Oxidative Stress II.* (Humana Press, 2010).

46. Ridley, A. J. *et al.* Cell migration: Integrating signals from front to back. *Science* **302,** 1704–1709 (2003).

47. Hood, J. D. & Cheresh, D. A. Role of integrins in cell invasion and migration. *Nat. Rev. Cancer* **2,** 91–100 (2002).

48. Scharffetter-Kochanek, K. *et al.* UV-induced reactive oxygen species in photocarcinogenesis and photoaging. *J. Biol. Chem.* **378,** 1247–1257 (1997).

49. Roca-Cusachs, P., Conte, V. & Trepat, X. Quantifying forces in cell biology. *Nat. Cell. Biol.* (2017).

50. Poirier, M. G. & Marko, J. F. Effect of Internal Friction on Biofilament Dynamics.

Phys. Rev. Lett. **88,** 228103 (2002).

51. Mizuno, D., Tardin, C., Schmidt, C. F. & MacKintosh, F. C. Nonequilibrium mechanics of active cytoskeletal networks. *Science* **315,** 370–373 (2007).

52. Vasconcellos, C. A. *et al.* Reduction in viscosity of cystic-fibrosis sputum in-vitro by gelsolin. *Science* **263,** 969–971 (1994).

53. Nakamura, F., Osborn, E., Janmey, P. A. & Stossel, T. P. Comparison of Filamin A-induced Cross-linking and Arp2/3 Complex-mediated Branching on the Mechanics of Actin Filaments. *J. Biochem.* **277,** 9148–9154 (2002).

54. Blanchoin, L. & Pollard, T. D. Interaction of actin monomers with acanthamoeba actophorin (ADF/cofilin) and profilin. *J. Biochem.* **273,** 25106–25111 (1998).

55. Püspöki, Z., Storath, M., Sage, D. & Unser, M. in *Focus on Bio-Image Informatics* **219,** 69–93 (Springer, Cham, 2016).

56. Boudaoud, A. *et al.* FibrilTool, an ImageJ plug-in to quantify fibrillar structures in raw microscopy images. *Nat. Protoc.* **9,** 457–463 (2014).

57. Wang, Z. *et al.* Long-term fluorescent cellular tracing by the aggregates of AIE bioconjugates. *J. Am. Chem. Soc.* **135,** 8238–8245 (2013).

58. Major, M. D. & Torkelson, J. M. Fluorescence of vinyl aromatic polyelectrolytes: effects of conformation, concentration, and molecular weight of sodium poly (styrene sulfonate). *Macromolecules* 2806–2810 (1986).

59. Ander, P. & Mahmoudhagh, M. K. Excimer formation of poly (styrenesulfonic acid) and its salts in solution. *Macromolecules* **15,** 214–216 (1982).

60. Yan, J. J. *et al.* Polymerizing nonfluorescent monomers without incorporating any fluorescent agent produces strong fluorescent polymers. *Adv. Mater.* **24,** 5617–5624 (2012).

61. Gerweck, L. E. & Seetharaman, K. Cellular pH gradient in tumor versus normal tissue: potential exploitation for the treatment of cancer. *Cancer Res.* **56,** 1194–1198 (1996).

62. Johnson, D. E., Ostrowski, P., Jaumouillé, V. & Grinstein, S. The position of lysosomes within the cell determines their luminal pH. *J. Cell Biol.* **212,** 677–692 (2016).

63. Bridges, J. W. & Williams, R. T. The fluorescence of indoles and aniline derivatives. *Biochem. J.* **107,** 225–237 (1968).

64. Goswami, T. K. *et al.* Ferrocene-conjugated copper(II) complexes of L-methionine and phenanthroline bases: synthesis, structure, and photocytotoxic activity. *Organometallics* **31,** 3010–3021 (2012).

65. Chen, S., Lu, J., Sun, C. & Ma, H. A highly specific ferrocene -based fluorescent probe for hypochlorous acid and its application to cell imaging. *Analyst* **135,** 577–582 (2010).

66. Kumar, K., Vulugundam, G., Kondaiah, P. & Bhattacharya, S. Co-liposomes of redox-active alkyl-ferrocene modified low MW branched PEI and DOPE for efficacious gene delivery in serum. *J. Mater. Chem. B* **3,** 2318–2330 (2015).

67. Vankayala, R., Kalluru, P., Tsai, H.-H., Chiang, C.-S. & Hwang, K. C. Effects of surface functionality of carbon nanomaterials on short-term cytotoxicity and embryonic development in zebrafish. *J. Mater. Chem. B* **2,** 1038–1047 (2014).

68. Blanazs, A., Ryan, A. J. & Armes, S. P. Predictive phase diagrams for RAFT aqueous dispersion polymerization: Effect of block copolymer composition, molecular weight, and copolymer concentration. *Macromolecules* **45,** 5099–5107 (2012).

69. Refojo, M. F. Hydrophobic interaction in poly(2-hydroxyethyl methacrylate) homogeneous hydrogel. *J. Polym. Sci. A* **5,** 3103–& (1967).
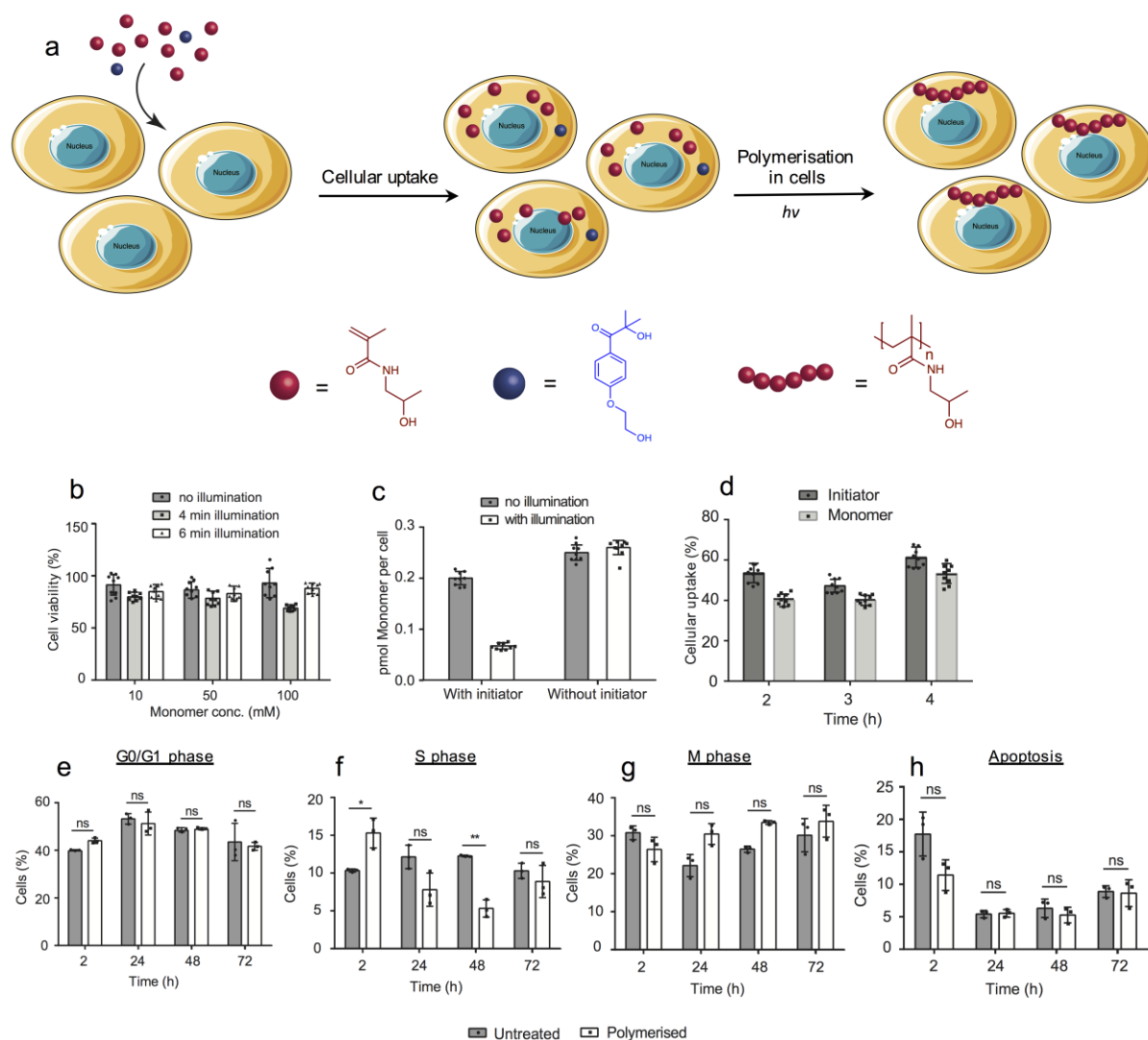
Figure 1. Intracellular polymerisation.

(**a**) Generic strategy for polymerisation inside living cells. The monomer *N*-(2-hydroxypropyl) methacrylamide (HPMA) and the initiator Irgacure 2959 were added to the cell culture, with photo-polymerisation initiated by illumination at 365 nm for 5 min. (**b**) HeLa cells were incubated with monomer HPMA (10, 50, and 100 mM) and initiator Irgacure 2959 (2 mM) for 4 h, followed by photo-polymerisation (4 or 6 min at 365 nm) and cell viability measured after 48 h (MTT assay, n = 3 independent experiments with 3 independent samples in each). An untreated population of HeLa cells, without illumination, was used to determine the relative cell viability, with cell viability > 85% for all concentrations of HPMA used (for cytotoxicity evaluation of Irgacure 2959, see Supplementary Fig. 17). (**c**) Time-dependent

cellular uptake of monomer and initiator (at 50 mM and 2 mM, respectively) after incubation with cells for 2, 3 or 4 h. Cells were washed, lysed, and monomer and initiator were extracted and quantified by HPLC, and displayed as percentages of initial concentrations added to the cell culture (n = 3 independent experiments with 3 independent samples in each). (**d**) Intracellular monomer concentration in the presence or in the absence of initiator after photo-polymerisation (5 min at 365 nm). Cells were washed, lysed, and monomer and initiator were extracted and quantified by HPLC (n = 3 independent experiments with 3 independent samples in each). (**e**) to (**h**) The cell cycle was investigated by treating the cells with the monomer (50 mM) and initiator (2 mM), followed by photo-polymerisation. Vybrant$^{®}$ DyeCycle^{TM} ($\lambda_{ex/em}$ = 488/534 nm) was used for dsDNA staining. The data is presented as mean ± SD (n = 3 independent samples for each group). Significant differences were analysed using two-way analysis of variance followed by Sidak's multiple comparison test compared to an untreated control group (ns, not significant, * $P = 0.049$, ** $P = 0.0063$).
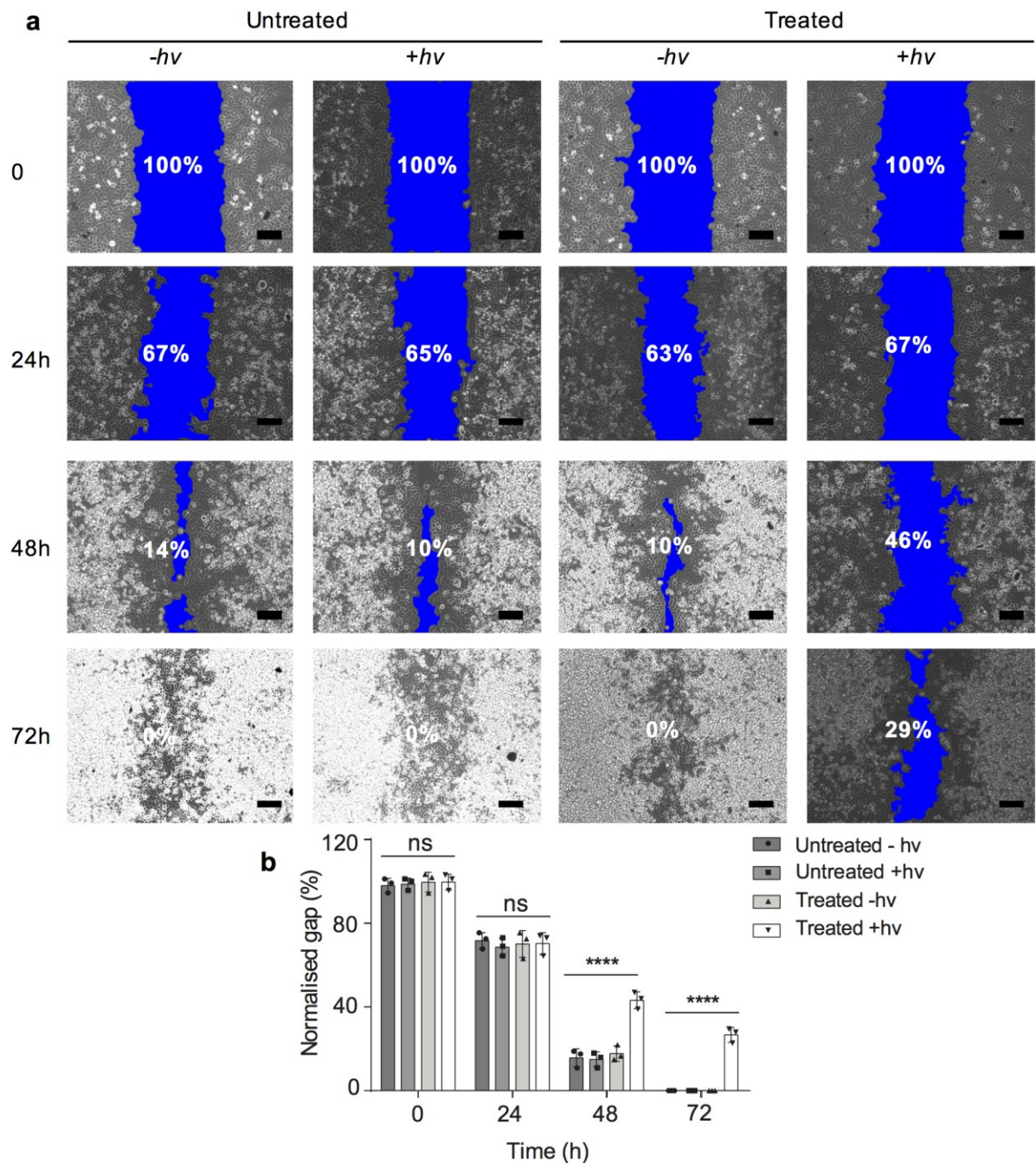
Figure 2. HeLa cells that underwent intracellular polymerisation were less migratory and actin cytoskeleton organisation was altered. (**a**) Cell migration was determined by a wound-healing assay of HeLa cell monolayers. HeLa cells were plated in an Ibidi® Culture-Insert 2 Well μ-Dish. Cells were treated with HPMA (50 mM) and Irgacure 2959 (2 mM) for 4 h, followed by illumination at 365 nm for 5 min. "Wounds" were created using Ibidi insert kits and "wound closure" was monitored by bright-field microscopy at 24 h, 48 h, and 72 h with untreated cells and treated cells with and without 5 min illumination at 365 nm. Wound

areas were measured using ImageJ and are coloured in blue. Scale bar = 100 μm. The experiments were repeated, independently, 3 times with similar results observed. (**b**) The normalised gaps *vs* time (calculated as the ratio of the remaining gap area at the given time point and at t = 0 h) (data represent the mean ± SD, n = 3 independent experiments). Significant differences were analysed using two-way analysis of variance followed by Sidak's multiple comparison test compared to an untreated control group (ns, not significant, **** $P < 0.0001$).
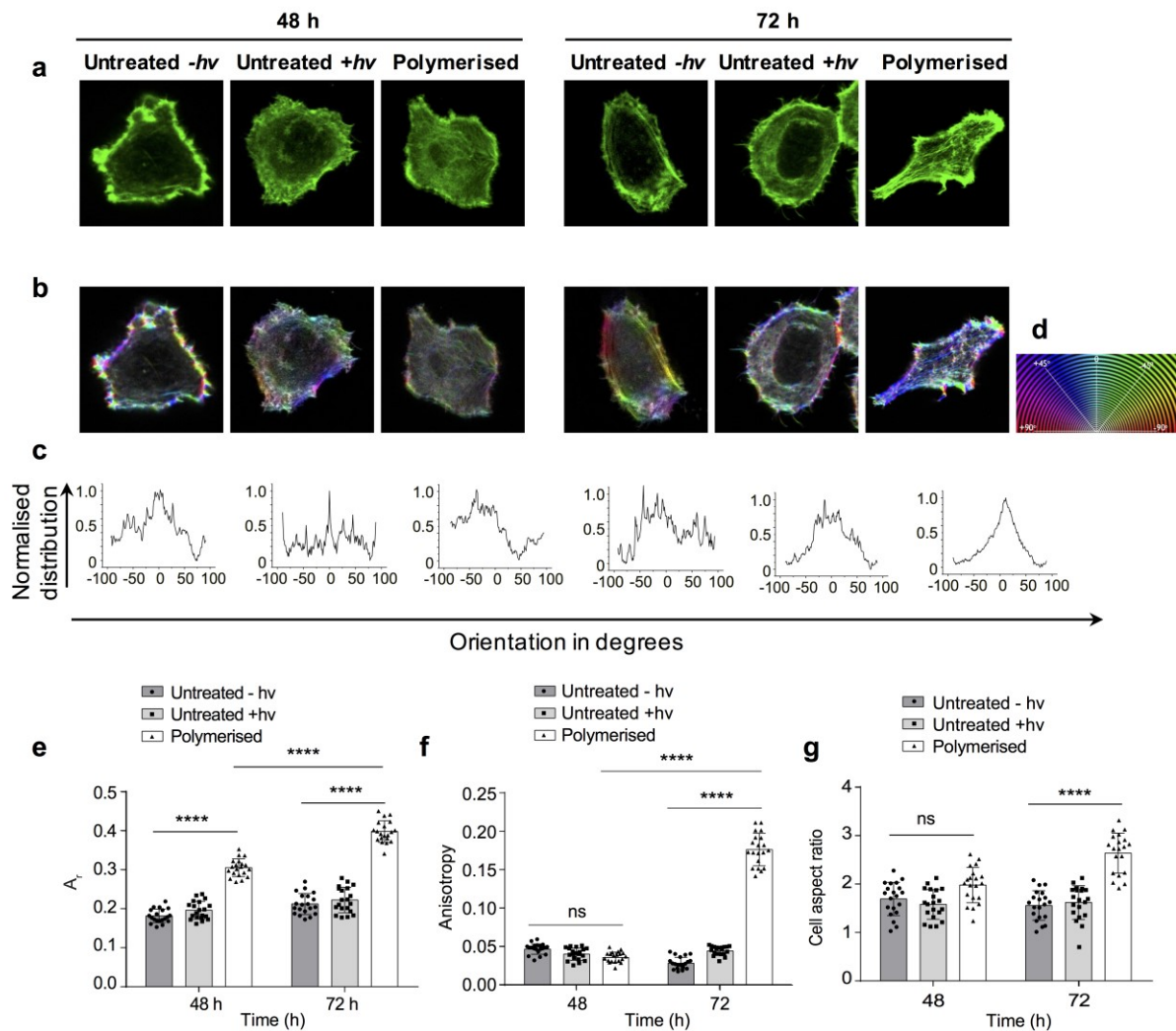
Figure 3. Actin cytoskeleton organisation was altered in polymerised HeLa cells.

(**a**) Untreated cells, with and without illumination, and polymerised cells (incubated with 50 mM HPMA and 2 mM Irgacure 2959 for 4 h, followed by 5 min at 365 nm) were stained for

actin filaments (F-actin, after removal of cellular membranes) after 48 h and 72 h. Scale bar = 10 μm. (**b** and **c**) Corresponding orientation plots for actin staining, where the different colours indicate different orientations of actin filaments, as per the given colour map (**d**). The experiments were repeated, independently, 3 times with similar results observed. (**e**) Area of actin microdomains relative to cell area (A_r) for untreated cells with and without illumination (5 min at 356 nm), and polymerised cells incubated for 48 h and 72 h (data represent the mean ± SD, with each data point corresponding to 20 cells.) (**f**) Quantitative analysis of the anisotropy of actin from confocal images of HeLa cells (n = 20 cells per condition, mean ± SD). (**g**) Aspect ratio of cell shape for untreated and polymerised cells after incubation for 48 h and 72 h. 20 cells were analysed for each experiment. (e)–(g) Significance was analysed by two-way analysis of variance followed by Sidak's multiple comparison test compared to untreated cells with and without illumination (ns, not significant, **** $P < 0.0001$).
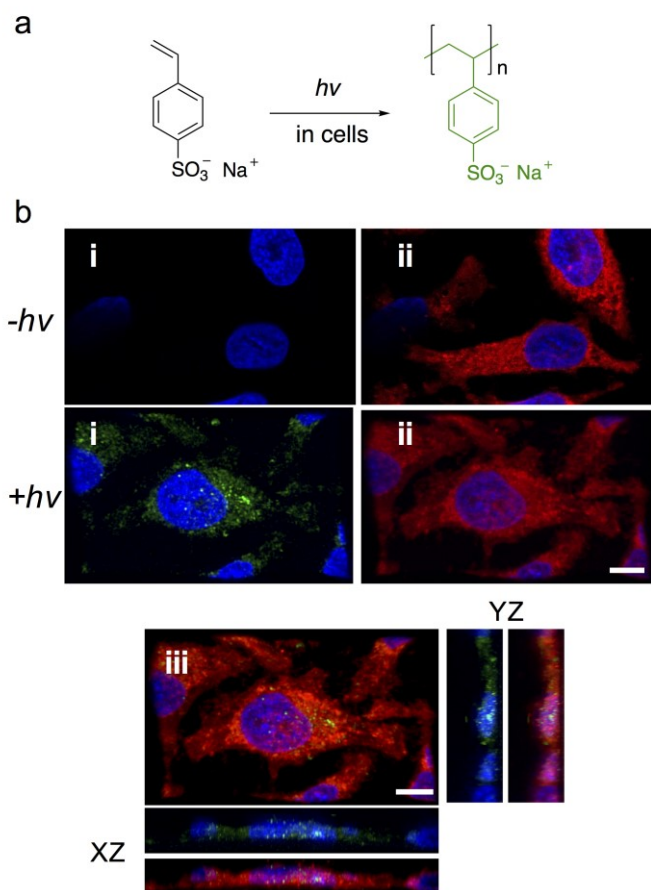
Figure 4. Polymerisation of sodium styrenesulfonate (NaSS) in HeLa cells.

(**a**) Polymerisation of NaSS in cells. (**b**) Confocal fluorescence microscopy images of HeLa cells, with and without illumination, showing the intracellular polymerisation of NaSS. Cell nucleus stained with Hoechst 33342 (blue, $\lambda_{ex/em}$ = 353/483 nm); Plasma membrane stained with CellMask^{TM} Deep Red (red, $\lambda_{ex/em}$ = 649/666 nm); poly(NaSS) (green, $\lambda_{ex/em}$ = 480/565 nm); (**i**) Merged image of nucleus and NaSS or poly(NaSS), (**ii**) Merged image of nucleus and cell membrane; (**iii**) Merged image of all channels and 3D confocal image (Z-stacks projection) showing polymerised NaSS inside the cell with a vertical cross-section through the cells (see also Supplementary Movie 1). Scale bar = 10 µm. The experiments were repeated, independently, 3 times with similar results observed.
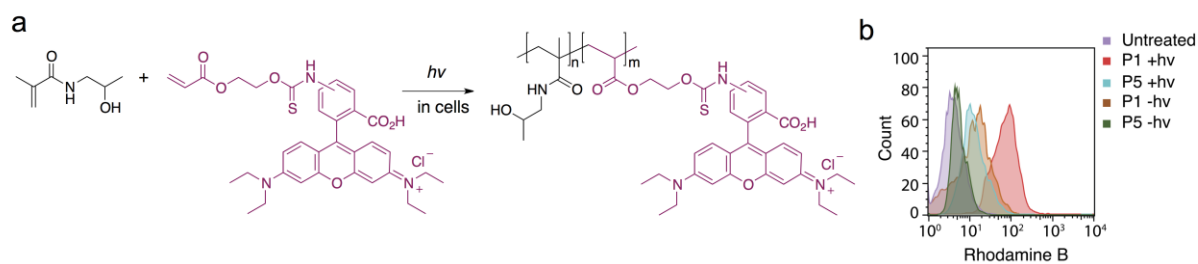
Figure 5. **Co-polymerisation of HPMA with acryloxyethyl thiocarbamoyl rhodamine B (AOTCRhB) in HeLa cells.** (**a**). Photo-polymerisation of HPMA (20 mM) and AOTCRhB (5 μM) in cells. (**b**) Flow cytometry analysis ($\lambda_{ex/em}$ = 536/617 nm) of intracellular poly(HPMA-*co*-AOTCRhB) at cell passages P1 and P5. After five passages, the fluorescence intensity naturally reduced; however, the "polymerised cells" still exhibited high fluorescence intensity when compared with non-polymerised cells. The experiments were repeated, independently, 3 times with similar results observed.
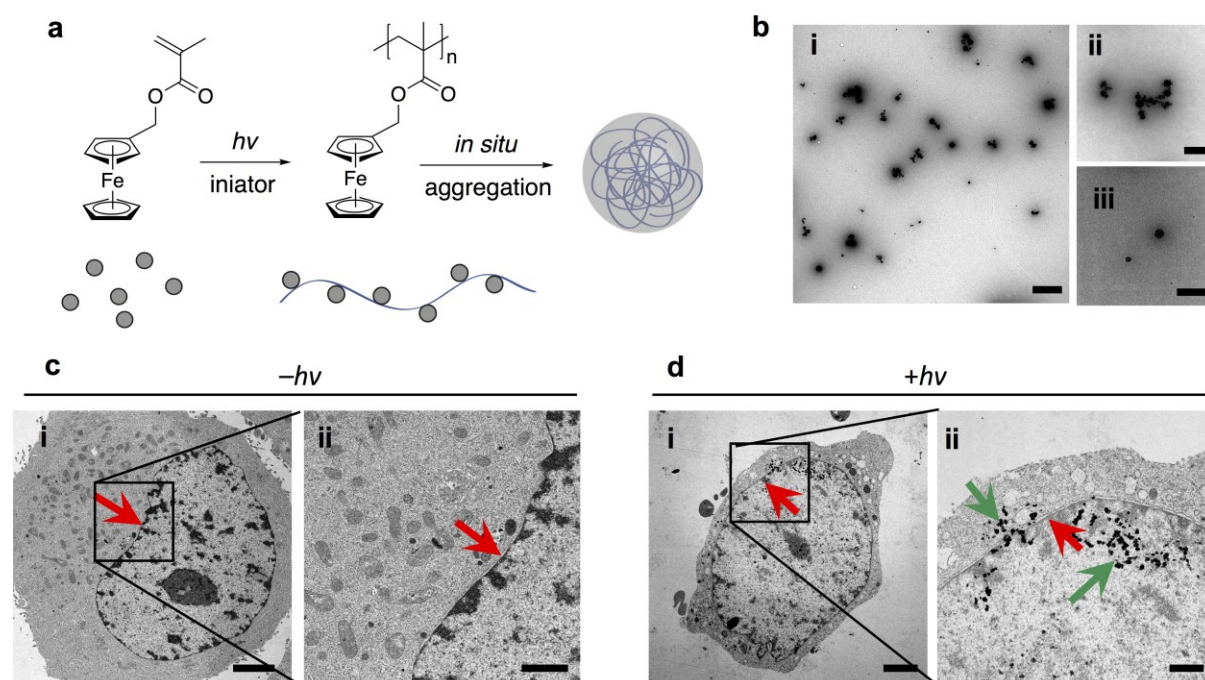

Figure 6. **Polymerisation of ferrocenylmethyl methacrylate (FMMA) in HeLa cells**.

(**a**) Photo-polymerisation of FMMA in the presence of initiator was followed by self-aggregation to form nanoparticles. (**b**) (**i**) TEM image of ferrocene polymeric nanoparticles

formed *in vitro*, showing both individual and small clusters of particles; **(ii)** Clusters of nanoparticles; **(iii)** Individual nanoparticles. Scale bars = (i) 1 µm; (ii) and (iii) 500 nm. **(c)** and **(d)** TEM images of HeLa cells incubated with FMMA (10 mM) and initiator (1 mM) without and with illumination (5 min at 365 nm), respectively. The cells were fixed, sliced, and treated with uranyl acetate to stain membranes and lead citrate to stain the nucleus. Ferrocene nanoparticles were located in the cytoplasm and the nucleus. Red arrows show the nuclear membrane and green arrows show the ferrocene nanoparticles. **(i)** A single cell and **(ii)** magnification of nuclear membrane. Scale bars: (c) (i) = 2 µm, (ii) = 500 nm; (d) (i) = 1 µm, (ii) = 500 nm. (b)–(d) The experiments were repeated, independently, 3 times with similar results observed.

Table 1. IC$_{50}$ values of monomers against HeLa cells (incubation for 48 h, MTT assay).

Monomer[a]	IC$_{50}$
HPMA	>250 mM
NaSS	>100 mM
VAN	56 mM
FMMA	68 mM
AEMA	20 mM
VBA	15 mM
MBA	20 mM
PEGDA (M_n = 575 Da)	4 mM
PEGDA (M_n = 10 kDa)	25 mM
AOTCRhB[b]	20 µM
Acrylamide[b]	1 µM
PEGMA (M_n = 480 Da)[b]	1 mM
HEMA[b]	7 mM
O-HPMA[b]	8 mM

[a]Abbreviations: HPMA (*N*-(2-hydroxypropyl) methacrylamide); NaSS (sodium 4-styrenesulfonate); VAN (4-vinylaniline); FMMA (ferrocenylmethyl methacrylate); AEMA (2-aminoethyl methacrylate); VBA (4-vinylbenzoic acid); MBA (*N,N ′*-methylenebis(acrylamide)); PEGDA (poly(ethyleneglycol) diacrylate); AOTCRhB (acryloxyethyl thiocarbamoyl rhodamine B); PEGMA (polyethylene glycol methyl acrylate); HEMA (2-hydroxyethyl methacrylate); *O*-HPMA (*O*-2-hydroxypropyl methacrylate).

Data availability

All relevant data are available with the manuscript, or in the Supplementary Information.

Author contributions

J.G. and M.B. conceived, designed, and directed the project. W.S.L., and Y.C.Z. conducted the control polymerisations and MTT assays, Y.C.Z. conducted the actin experiments, Y.C.Z. and N.T. conducted the wound healing experiments, W.S.L., Y.C.Z., and J.C. conducted the fluorescent polymers. J.G., A.L. and M.B. co-wrote the manuscript. All authors analysed the data and contributed to the scientific discussion and revised the manuscript. J.G, Y.C.Z., and W.S.L. contributed equally to this work.

Competing interests

The authors declare no competing interests.